ASTRONOMY & ASTROPHYSICS
SUPPLEMENT SERIES

Astron. Astrophys. Suppl. Ser. **91,** 237-258 (1991)

A 257 – 273 GHz spectral survey of the OMC1 cloud core

J.S. Greaves[1] and Glenn J. White[1]

[1] Department of Physics, Queen Mary and Westfield College (University of London), Mile End Road, LONDON E1 4NS, U.K.

Received March 21, 1990; accepted April 17, 1991

Abstract. — A spectral line survey of the OMC1 cloud core has been obtained, over the frequency range 257.04 – 273.02 GHz, using the James Clerk Maxwell 15 m sub-millimetre telescope. Additional observations have been made centred at 229.4, 231.2, 237.3 and 239.1 GHz. A new algorithm was used to deconvolve the original double-sideband data, and its performance is critically discussed.

181 distinct spectral lines were detected, ~ 7 of which are not identifiable with known molecular transitions. Between 18 and 21 molecular species were detected, including up to 10 isotopically-substituted forms. The line strengths are greater by a factor of 1.9 (on average) than in an earlier OVRO survey of similar frequencies, made using a larger beam. The current results therefore provide a substantial database of typical line strengths for future high-resolution studies of the OMC1 core.

Key words: data analysis — interstellar medium: clouds: OMC1 — interstellar medium: molecules.

1. Introduction.

The core of OMC1 (Orion Molecular Cloud 1) contains one of the most interesting nearby examples of a high-mass star formation region, in terms of both chemistry and dynamics. At least 40 distinct molecular species have been detected, including ions, radicals, carbon-chains and complex, chemically-saturated molecules. These species are located in several regions, with varying temperature and velocity, all contained within a cloud core only ~ 0.05 pc in diameter.

Infra-red studies of the cloud core have detected several bright embedded sources, with total luminosity $L \sim 10^5\ L_\odot$ (e.g. Wynn-Williams *et al.* 1984). Of these, IRc2, the source of most of the luminosity, appears to be the origin of the bipolar outflow, but the highest velocity material is located a few arcseconds to the north (Wilson *et al.* 1986). A torus oriented approximately perpendicular to the flow direction has been detected in SO by Plambeck *et al.* (1982). This disk does not appear to be the only influence controlling the outflow morphology, since the lobes are highly asymmetric. Also important are the clumpy hot core (containing most of the nitrogen-rich species), centred 2″ – 3″ south of IRc2, and the ambient cloud material. This gas (containing most of the ions and radicals) forms part of an extended N – S ridge which passes through the core. Close to IRc2,≈10" to the south, there is another distinct ridge region, known as the "compact ridge" (Plambeck & Wright 1987). This is similar in velocity and lindewidth to the extended ridge, but is warmer, and contains more oxygen-rich species (Blake *et al.* 1987).

Many observations have been made of the molecular gas components, in order to understand the complex chemistry of the cloud core. Previous molecular surveys include those of Johansson *et al.* (1984) (72 – 91 GHz), Turner (1989) (70 – 115 GHz), Sutton *et al.* (1985) (215 – 247 GHz) and Blake *et al.* (1986) (247 – 263 GHz). The present survey, using the JCMT 15 m telescope, covers the frequency range 257 – 273 GHz (plus a few parts of the 229 – 239 GHz region). Thus it extends the frequency range previously covered, and also allows comparisons to be made with the strengths of lines previously observed by Sutton *et al.* (1985) and Blake *et al.* (1986), using the OVRO 10.4 m telescope. In addition, the current high angular resolution (19″, compared to $\gtrsim$ 30″ previously) results in less beam-dilution, and hence can provide better estimates of the cloud core abundances.

2. Observations.

The observations were obtained during October 1988, using the 15 m James Clark Maxwell Telescope (JCMT), situated on Mauna Kea, Hawaii, with some additional observations during September 1989. The receiver system consisted of a Schottky-diode mixer used in conjunction with an acousto-optical spectrometer (AOS). System noise temperatures in October 1988 were 1000 – 3000 K (double-

sideband), with the higher values occuring at higher frequencies, and in September 1989 the system temperatures were 800 – 1100 K. Sky opacities were typically ~ 0.1. Integration times were 5 – 15 minutes, including on and off source positions.

The central position used was Right Ascension (1950) = 05h 32m 47s, Declination (1950) = −05° 24′ 26″ (centred on the hot core, 2″ south of IRc2), with pointing errors of 1″ – 5″ at 257 – 273 GHz and 3″ – 7″ at 229 – 239 GHz. (The pointing errors were measured from available planets, and represent the amount of drift since the previous correction.) The observations were made by position switching, to reference points located ≈ 1° north. The beamsize of the JCMT at 265 GHz was FWHM = 19″, and at a distance ~ 500 pc (Genzel *et al.* 1981) this is equivalent to a spatial resolution of 0.05 pc. (At 230 GHz, the beamsize was FWHM = 21″.) The survey is presented in the form of corrected antenna temperature $T_R^* (= T_A^*/\eta_{fss})$ (Kutner & Ulich 1981). The forward spillover and scattering efficiency η_{fss} was estimated to be 0.75 at 257 – 273 GHz, and 0.73 at 229 – 239 GHz, with errors in η_{fss} ~ 10%.

No corrections have been made for coupling of the beam to the source, but this will be less than unity for the hot core, outflow and ridge regions, since they do not fill the beam. For sources which do not extend beyond the telescope sidelobes, the coupling efficiency η_c is given approximately by $\sigma_s^2/(\sigma_s^2+\sigma^2)$, where σ_s and σ are the Gaussian radii of the source and beam respectively. Hence, for σ = 8.5″ (FWHM = 20″), and a typical σ_s of ~ 5″, η_c ~ 0.25. Corrections to the line strengths from pointing offsets have also been omitted, but these are small for most of the lines. For sources located near the beam centre, a 5″ pointing change results in a difference in T_R^* of ≤ 20% (decreasing error with increasing source size). The corrections are substantial only for transitions from the compact ridge, located ≈ 10″ from the JCMT beam centre, where the line strengths are a factor of 2 less than if the source had been at the beam centre, and a 5″ pointing offset changes the intensities by another factor ~ 2. Thus the smaller beam used for this survey has resulted in larger η_c values than previous studies, but there is a loss of sensitivity to the compact ridge emission.

3. Data reduction.

During the 1988 observations, a series of spectra were obtained whose centre frequencies were spaced by 475 MHz, covering the spectral range 265 – 273 GHz in double-sideband (DSB) mode. A second independent set of spectra was then obtained, with centre frequencies offset by 20 MHz relative to the first set. This frequency offset resulted in a shift of the image, lower, sideband (LSB) lines, relative to the upper-sideband (USB) lines. Thus each spectral line in this range is identifiable as a USB or LSB feature. The intermediate frequency used was 3.94 GHz, giving a separation of 7.88 GHz between the USB and LSB centres, hence observations at 264.90 – 273.02 GHz in DSB mode gave complete coverage of the spectral range 257.04 – 273.02 GHz. The additional observations (in September 1989) were made using the same offset technique, and the final frequency range covered was 229.17 – 229.64, 230.98 – 231.44, 237.06 – 237.54 and 238.86 – 239.34 GHz.

The single-sideband (SSB) spectrum is presented in Figure 1, with the channels binned to a resolution of 2 MHz (corresponding to 2.2 – 2.6 km s^{-1}). The DSB data was deconvolved using a new algorithm described in Appendix A. This is based on the fact that a USB line will be blended with a different region of the LSB spectrum when the local oscillator frequency, and hence the passband centre frequencies, are increased by 20 MHz (Fig. 2). This enables the antenna temperature contributions from the two sidebands to be separated.

The rms noise of the SSB spectrum is approximately half that of the DSB spectrum. This apparent reduction in the noise is an artefact of the deconvolution process, since where several solutions to the equations are possible (more than one DSB value is within the noise), the solution with the minimum, absolute, value is chosen. The choice of a particular solution is entirely arbitrary, since they differ only by the noise on the DSB antenna temperatures. The minimum solutions were used to reduce the number of spurious features (spikes) and to ensure that weak lines were real. (A rejection procedure was included in the algorithm to prevent the subtracting of positive spikes from a baseline region). The form of the algorithm used here was such that a peak line temperature may be underestimated by at most three times the noise level (see Appendix A).

This method of data reduction relies on the presence of featureless regions of the spectrum. Where parts of the spectrum are confusion-limited, so that spectral lines were detected in all n channels involved in the algorithm, no solutions to the equations can be found. For the current survey, ≈ 96% of the channels were solvable, with a further ≈ 3% solved by averaging over the two immediately adjacent SSB channels. Thus only ≈ 1% of the spectrum is unsolved, and for these channels T_R^* has been set to zero. These regions are indicated in Figure 1.

A problem with the earlier data arose from the fact that ≈ 100 MHz at one end of the AOS was much noisier than the centre, by a factor ≈ 4 – 5. These noisy regions are apparent in Figure 1, e.g. at 259.46 to 259.57 GHz. Spectra at the noisy end occasionally has worse baselines, hence the intensities of a line located at a scan edge differed by up to ~ 5 K in the offset scans. This has resulted in spikes in the SSB spectrum, where antenna temperature solutions in adjacent channels have been taken from the two different scans. These regions are also indicated in Figure 1.

Some problems were experienced with the frequency-calibration of both the AOS used. After the observations were completed, it was discovered that the AOS frequency calibration was subject to drifts of ≲ 10 km s^{-1}, and that

the frequency calibration curve was not the same from night to night. Frequency corrections ($\sim$ 1 MHz in size) have been made (as far as possible) in the DSB to SSB deconvolution, using offsets measured from a reference signal moved in 40 MHz increments across the passband. These frequency deviations had amplitudes which followed an approximately sinusoidal pattern, with one or two periods over the 500 MHz passbands (1988 and 1989 observations respectively). However, since the calibration drifted over the observing periods, and the offsets were only measured once, these corrections were insufficient to eliminate the frequency anomalies. The maximum remaining error is $\sim$ 8 MHz.

The frequency errors do *not* affect the SSB line widths or intensities, since the deconvolution uses DSB antenna temperatures from channels spaced only 40 MHz apart. Over these limited regions the measured *differences* in the frequency offsets were $\leq$ 1 MHz, less than the 2 MHz channel width, hence the separation of the lines is negligibly affected, and only the derived velocities are wrong, not the line shapes. The velocities of the line peaks have therefore been omitted from the tables. The line identifications are not affected, since most possible associations within a few MHz of the line wings have been listed. The exceptions (omitted identifications) are transitions with $E_u/k > 600$ K or very small intrinsic strength S_{ij}; species whose transitions were *only* found associated with other possible identifications; and associations where other, unblended, transitions of similar predicted strength (similar $E_u/k, S_{ij}$) were not detected. Consequently there is little doubt the line identifications, but the rest frequencies of the $U-$lines are uncertain by $\lesssim$ 8 MHz. For a particular $U-$line, the frequency offset can be estimated by comparison with nearby identified lines.

4. Results.

152 spectral lines at 257 – 273 GHz, and 29 lines in the range 229 – 239 GHz, are present in the deconvolved survey presented in Figure 1. (The molecules detected are listed in Table 1, with the transitions observed in Table 2, and measurements of the peak antenna temperatures and line widths are presented in Table 3. The molecular identifications have mostly been made from the catalogue of Lovas 1984). There are definite detections of 18 distinct molecular species, with tentative detections of a further 3 molecules. The latter class consists of detections with poor signal-to-noise ratios, or molecules where the transitions observed lie at similar frequencies to transitions of a second species. This occurs in cases such as H_2CO at 258,296 MHz, which is blended with $HCOOCH_3$. The total number of distinct molecules detected in OMC1 in surveys at 70 – 273 GHz (Johansson *et al.* 1984, Sutton *et al.* 1985, Blake *et al.* 1986, Turner 1989) is now $\approx$ 40, hence the JCMT survey provides a useful database of typical line strengths for approximately half the species identified.

TABLE 1. *Molecules detected in the spectral survey.*

molecule size	definite detections	tentative detections
2 atoms	^{13}CS, SO, SiO, ^{29}SiO	
3 atoms	SO_2, $^{34}SO_2$, OCS, HCN, $H^{13}CN$, $HC^{15}N$, HNC, $HN^{13}C$, CCH, HCO^+, HDO	$OC^{34}S$, $H^{13}CO^+$, $HC^{17}O^+$
4 atoms	H_2CS	H_2CO, NH_2D
5 atoms	HC_3N, CH_2CO	$H^{13}CCCN$, C_3H_2
6 atoms	CH_3CN, $^{13}CH_3CN$, CH_3OH	
7 atoms		
8 atoms	$HCOOCH_3$	
9 atoms	C_2H_5CN, CH_3OCH_3	

Many unidentified lines (U – lines) have been observed in OMC1, with up to 25 present in the current survey (Table 3.6). Some of these features may have resulted from deconvolution errors, where the baseline level is uncertain. Assuming that $U-$lines will be pseudo-randomly distributed throughout the survey, it is possible to estimate the number of these features that will coincide with a known transition in the other sideband (OSB). Of the 21 $U-$lines in the 257 – 273 GHz survey range, only 3 might be expected to do so, whereas there are in fact 17 coincidences. Thus a substantial number ($\sim$ 14/21 or two thirds) of these features may be artefacts of the deconvolution process. The 4 $U-$lines which do not coincide with an OSB feature are those at 259308, 265630, 266386 and 270664 MHz. Of the 10 $U-$lines lying in the 257 – 263 GHz region of the Blake *et al.* (1986) survey, which overlaps the current survey, four could not be detected due to excess noise, two were confirmed, two were identified with transitions of $HCOOCH_3$, and the remaining two lines (T_R^*(max) $\sim$ 1 K) were not confirmed.

All the molecules detected in this survey were already known to exist in OMC1. (The transition at 259,308 MHz was tentatively identified with SiCC $4_{2,2} - 3_{0,3}$, but a subsequent search for SiCC transitions with larger intrinsic strengths was not successful (Greaves *et al.* 1991a), hence this line remains unidentified.) The survey thus confirms that, while unidentified molecules are present in OMC1, they are not species so far predicted by current chemical models.

The smaller beam of the JCMT (FWHM = 19″, compared to the OVRO FWHM $\approx$ 30″) has resulted in less beam dilution, and enhancement of the majority of line strengths. The ratio of line intensities T_R^*(max) (JCMT)/ T_R^*(max) (OVRO), denoted by $R_{J:O}$, ranges from 0.7 – 3.2,

with an average value of 1.9, for unblended lines detected in both surveys. Examples of spectra with different values of $R_{J:O}$ are presented in Figure 3. In this part of the spectrum, stronger lines of SO_2, CH_3OH and C_2H_5CN were observed with the JCMT, but CCH was stronger in the OVRO survey, while the CH_3OCH_3 transition was not detected with the OVRO telescope. Over the 257 – 263 GHz region, wide ranges of $R_{J:O}$ were found using different transitions of each molecule, due to the noise levels, so characteristic values for each species were not generally observed, but $R_{J:O}$ was unusually low for CCH (≈ 0.7).

5. Discussion.

A more detailed discussion, including comparison with data at other frequencies, will be presented in a later paper (Greaves *et al.* 1991b). Preliminary analysis has shown that the line strengths are enhanced by use of a smaller beam, while the linewidths are similar to those reported from previous surveys (Blake *et al.* 1987, Johansson *et al.* 1984). The velocity extents of the outflow gas are also close to those found previously, with full widths at zero power up to 74 km s^{-1}. The FWZP values are similar for observations with different sized beams (shown by direct comparison of transitions observed both in the current survey, and by Blake *et al.* 1986). This implies that the high-velocity material is close to IRc2, since it lies within the 19″ JCMT beam.

The survey data has been used to estimate the fraction of the emission from the OMC1 core that occurs in spectral lines. The total integrated intensity of spectral line emission is $\approx 1.0 \times 10^4$ K MHz, in the 257 – 273 GHz range. (Some flux in weak lines will have been missed, but this effect is estimated to be small. The flux from lines of any particular $T_R^*(\max)$ is roughly constant, and only lines with $T_R^*(\max) \lesssim 2$ K have been missed. Even if the passband were filled with undetected lines at the average rms noise level of $T_R^* \approx 0.5$ K, the additional line flux would be only $\sim 8 \times 10^3$ K MHz). The strength of the continuum has not been measured at 257 – 273 GHz (1.1 – 1.2 mm), but can be estimated from results at other wavelengths. Sutton *et al.* (1984) used 400 μm – 1 mm data in a 36" beam, and found a spectral index of 2.7, which gives an extrapolated peak flux of 100 Jy at 1.1 mm. More recent results, with higher spatial resolution, include those of Mezger *et al.* (1990) (66.7 Jy at 1.3 mm, 21″ resolution) and White *et al.* (1991) (243 Jy at 800 μm, 15″ resolution). These results lie very close to the best fit of Sutton *et al.* (1984), indicating little variation in measured flux over this range of beam-sizes. Hence, adopting a peak flux of 100 Jy within a 19″ beam, the continuum strength is equivalent to $T_R^* = 4.7$ K, giving a total integrated intensity of 7.5×10^4 K MHz over the 257 – 273 GHz range.

The detected spectral line emission thus constitutes $\sim$ 10% of the total emission from the core, in the 1.1 – 1.2 mm region. This is considerably less than the 30 – 40% found by Sutton *et al.* (1984), using spectral survey data at 1.3 mm, from the OVRO 10.4 m telescope. Those results were based on a beam-filling correction, with an assumed source size $\sim$ 20″. Values of the spectral line to total emission as high as 40% can be obtained from our data, assuming a typical source size $\sim$ 10″ (observed for the hot core and compact ridge), but since the filling factor of the continuum emission is unknown, corrections to the line-to-continuum ratio are highly uncertain. However, the results indicate that care must be taken, when making broad-band measurements of the OMC1 continuum emission, to correct for the flux contribution from spectral lines.

6. Conclusions.

A molecular line survey of the OMC1 cloud core has been made, and $\approx$ 99% spectral coverage of the frequency range 257 – 273 GHz has been obtained. Additional observation have been made in the 229 – 239 GHz region. 181 distinct spectral features have been detected, of which $\sim$ 7 are from unidentified molecules. Between 18 and 21 known, molecular species were detected, with up to 10 isotopically-substituted forms also present. The line strengths are in general enhanced relative to the results from the OVRO survey (made with a larger beam size), hence the abundances of molecular species in the OMC1 core will need to be revised.

Acknowledgements.

We are grateful to Dr. Ed Sutton for providing a computer-readable version of the OVRO survey data, and to the referee Dr. M. Guélin for useful comments which helped to improve aspects of the paper. We also thank the staff at the JCMT for their support at the telescope, and the UK Science and Engineering Research Council for travel funding, the support of millimetre and sub-millimetre astronomy at Queen Mary and Westfield College, and a studentship for JSG. The JCMT is operated by the Royal Observatory, Edinburgh, on behalf of the SERC, the Netherlands Organisation for Pure Research and the National Research Council of Canada.

Appendix A

The DSB data were deconvolved to an SSB spectrum using a new deconvolution algorithm. Since this is of general use, it will be described here in detail.

For the observations presented here, the observing sideband was the USB, and the equations below are for this case. The frequency offsets $\Delta\nu$ are all for displacement measured

from the USB centre frequency. Similar equations can be formulated for observations in the LSB.

For passbands centered at ν_C,

$$\nu_C = \nu_{LO} \pm \nu_{IF} \quad (1)$$

where ν_{LO} is local oscillator frequency, and ν_{IF} is the intermediate frequency. A spectral line of rest frequency ν_0 will be observed at an offset $\Delta\nu$ from ν_C, where $\Delta\nu$ is given by

$$\Delta\nu = \nu_0 (1 - (v_e + v_s)/c) - \nu_{USBC} \quad (2)$$

for a USB line, where ν_{USBC} is the USB centre frequency, and by

$$\Delta\nu = -\nu_0 (1 - (v_e + v_s)/c) + \nu_{USBC} - 2\nu_{IF} \quad (3)$$

for a LSB line. The velocity of the source relative to the local standard of rest, lsr, is given by v_s. The velocity of the observer, on a line of sight to the source, relative to the lsr, is given by v_e, and consists of the sum of components from rotation and orbital motion of the earth, and the movement of the sun relative to the lsr. The usual convention has been used, i.e., motion of the observer away from the source gives $v > 0$.

For a channel with a frequency ν_U in the USB range, the observed DSB antenna temperature T_R^* is given, for the *first* set of scans, by

$$T_R^*(\mathrm{DSB}) = T_1(\nu_U) = T(\nu_L) + T(\nu_U). \quad (4)$$

$T(\nu_L)$ and $T(\nu_U)$ are the antenna temperature contributions (in T_R^* form) from the LSB and USB, at frequencies ν_L and ν_U respectively, where ν_L is the LSB frequency giving the *same value of* $\Delta\nu$ *as* ν_U.

For the *second* set of scans, at the same ν_U,

$$T_R^*(\mathrm{DSB}) = T_2(\nu_U) = T(\nu_L + 2\delta\nu) + T(\nu_U) \quad (5)$$

where $\delta\nu$ is the frequency offset between the two surveys, here 20 MHz.

By considering the LSB frequency, ν_L, as fixed, instead of ν_U, and finding the two different USB contributions from the two scans, another equation can be found:

$$T_R^*(\mathrm{DSB}) = T_3(\nu_U + 2\delta\nu) = T(\nu_L) + T(\nu_U + 2\delta\nu). \quad (6)$$

This process can be continued by considering other frequencies introduced above, eg. $\nu_U + 2\delta\nu$, and a set of n equations in $(n+1)$ unknowns (values of $T_R^*(\mathrm{DSB})$) results. Solutions are found as follows. If, for example, $T_1(\nu_U) < 2\sigma$ noise level, $T(\nu_U)$ and $T(\nu_L)$ are then both likely to be noise, and can be set to a convenient values, such as T_1. There are now $(n-1)$ equations remaining, in $(n-1)$ unknowns, hence antenna temperature solutions for all the frequencies involved can be found.

The higher the density of spectral lines, the larger the number of equations that is required to include a frequency free of transitions. For the current survey, $n = 5$ was used. No significant increase in the number of channels solved was found for larger values of n. Only solutions where DSB antenna temperatures enter up to three times were used (eg $T_R^*(\mathrm{SSB}) = T_1$, or $T_1 - T_2$, or $T_1 - (T_2 - T_3)$), to reduce the amount of noise included in the solution.

Since the noise level of the AOS was variable, being greater at the high-frequency end, several values of the 2σ noise were used. Solutions were searched for with successively higher values ($T_R^* = 1$, 2 and 3 K) used as the cutoff point. This has led to a few spurious solutions, apparent in Figure 1 as abrupt changes in line profile.

The relative gain ratio of the two sidebands has been estimated at 1.0 ± 0.1 (P. Friberg, private communication). This is therefore not a major factor influencing the line strengths, and has been omitted from the DSB separation routine. Also omitted are the effects of the variation of sky opacity with frequency, estimated from atmospheric models to be $\lesssim 10\%$.

References

Blake G.A., Sutton E.C., Masson C.R., Phillips T.G. 1986, ApJS 60, 357
Blake G.A., Sutton E.C., Masson C.R., Phillips T.G., 1987, ApJ 315, 621
Genzel R., Reid M.J., Moran J.M., Downes D. 1981, ApJ 244, 884
Greaves J.S., White G.J., Parker N.D. 1991a (in preparation)
Greaves J.S., White G.J., Bakes E.L.O.: 1991b (in preparation)
Johansson L.E.B., Andersson C., Elldér J., Friberg P., Hjalmarson Å, Höglund B., Irvine W.M., Olofsson H., Rydbeck G. 1984, A&A 130, 227
Kutner M.L., Ulich B.L. 1981 ApJ 250, 341
Lovas F.J. 1984, SLAIM magnetic tape version I-84, priv. comm.

Mezger P.G., Wink J.E., Zylka R. 1990, A&A 228, 95
Plambeck R.L., Wright M.C.H., Welch W.J., Bieging J.H., Baud B., Ho P.T.P., Vogel S.N. 1982 ApJ 259, 617
Plambeck R.L., Wright M.C.H. 1987, ApJ 317, L101
Sutton E.C., Blake G.A., Masson C.R. Phillips T.G. 1984, ApJ 283, L41
Sutton E.C., Blake G.A., Masson C.R., Phillips T.G. 1985 ApJS 58, 341
Turner B.E. 1989, ApJS 70, 539
White G.J., Padman R., Richardson K.J., Webster A.S., Parker N.D. 1991, A&A (submitted)
Wilson T.L., Serabyn E., Henkel C. 1986, A&A 167, L17
Wynn-Williams C.G., Genzel R., Becklin E.E., Downes D. 1984, ApJ 281, 172

TABLE 2. *Transitions observed. The level are given in* J, J_K, J_{K_{-1},K_1} *or (N,J) notation, with the hyperfine values (F) if applicable.* E_u/k, ν_0 *and* S_{ij} *are the energy above the ground state of the upper level of the transition, the rest frequency, and the intrinsic strength of the transition, respectively. A range of* ν_0 *values is given where several fine structure components of a transition are blended together, and the* S_{ij} *values are summed. Unidentified transitions are denoted by* U, *or* (U) *where they are coincident with an OSB feature (see text).*

ν_0 (MHz)	molecule	transition	symmetry state	values of F	E_u/k (K)	S_{ij}
229260.2	$HCOOCH_3$	$23_{9,14} - 23_{8,15}$	E		217	11.8
229265.2	C_2H_5CN	$26_{2,25} - 25_{2,24}$			154	25.8
229319.2	$HCOOCH_3$	$23_{9,15} - 23_{8,16}$	E		217	11.8
229347.7	SO_2	$11_{5,7} - 12_{4,8}$			122	1.2
229388.9	$HCOOCH_3$	$23_{9,15} - 23_{8,16}$	A		217	11.8
229405.0	$HCOOCH_3$	$18_{3,15} - 17_{3,14}$	E		111	17.3
229420.2	$HCOOCH_3$	$18_{3,15} - 17_{3,14}$	A		111	17.3
229590.4 – 229595.1	$HCOOCH_3$	19 – 18	E		117	21.6
229595.1	$HCOOCH_3$	$19_{3,17} - 18_{2,16}$	A		117	10.8
231061.0	OCS	19 – 18			111	19.0
231220.8	^{13}CS	5 – 4			33	5.0
231232.1 – 231239.1	$HCOOCH_3$	29 – 29 and 21 – 21	E		190 – 265	19.3
231266.0	(U)					
231281.1	CH_3OH	$10_2 - 9_3$	A–			
231310.4 – 231313.2	C_2H_5CN	26 – 25, 27 – 26, 24 – 23			153	61.2
231315.4	$HCOOCH_3$	$29_{4,26} - 29_{3,27}$	A		264	9.0
231342.0	(U)					
231412.2	$HCOOCH_3$	$35_{10,25} - 35_{9,20}$	A		441	20.8
237068.8	SO_2	$12_{3,9} - 12_{2,10}$			94	6.9
237170.3	$^{34}SO_2$	$25_{8,18} - 26_{7,19}$			449	3.3
237170.4	C_2H_5CN	$26_{3,23} - 25_{3,22}$			162	25.7
237288.0	(U)					
237297.0 – 237297.5	$HCOOCH_3$	13 – 12 and 20 – 19	E		65 – 128	23.3
237306.0 – 237309.5	$HCOOCH_3$	20 – 19 and 21 – 20	A and E		128 – 131	39.8
237338.1	C_2H_5CN	$14_{2,12} - 13_{0,13}$			50	0.02
237344.9	$HCOOCH_3$	$21_{1,20} - 20_{1,19}$	E		131	20.5
237393.2 – 237398.6	$HCOOCH_3$	$21_{2,20} - 20_{1,19}$	A and E		131	32.6
237405.2	C_2H_5CN	$26_{2,24} - 25_{2,23}$			158	25.8
237430.9	$HCOOCH_3$	$8_{3,6} - 7_{1,7}$	A		27	0.02
237476.1	C_2H_5CN	$25_{2,24} - 24_{1,23}$			143	13.1
238912.7	CH_3CN	$13_7 - 12_7$			428	9.2
238972.4	CH_3CN	$13_6 - 12_6$			336	10.2
238992.6	SO_2	$21_{7,15} - 22_{6,16}$			332	2.7
239022.9	CH_3CN	$13_5 - 12_5$			258	11.1
239046.0	(U)					
239064.3	CH_3CN	$13_4 - 12_4$			194	11.8
239096.5	CH_3CN	$13_3 - 12_3$			144	12.3
239119.5	CH_3CN	$13_2 - 12_2$			109	12.7
239133.3	CH_3CN	$13_1 - 12_1$			87	12.9
239137.9	CH_3CN	$13_0 - 12_0$			80	13.0

TABLE 2. *(continued)*

ν_0 (MHz)	molecule	transition	symmetry state	values of F	E_u/k (K)	S_{ij}
257100.0	SO_2	$7_{3,5} - 7_{2,6}$			48	3.5
257103.6	C_2H_5CN	$28_{2,27} - 27_{1,26}$			177	16.2
257106.4	C_2H_5CN	$30_{1,29} - 29_{2,28}$			202	18.2
257188.0	(U)					
257210.7	CH_3CN	$14_8 - 13_8$			547	3.1
257239.9	C_2H_5CN	$30_{1,30} - 29_{1,29}$			193	29.9
257252.6	$HCOOCH_3$	$20_{5,15} - 19_{5,14}$	A		143	18.8
257255.0	^{29}SiO	6 – 5			43	6.0
257284.8	CH_3CN	$14_7 - 13_7$			440	3.5
257349.1	CH_3CN	$14_6 - 13_6$			348	3.8
257402.2	CH_3OH	$18_{3,} - 18_2$	A+ –			
257403.6	CH_3CN	$14_5 - 13_5$			270	12.2
257448.1	CH_3CN	$14_4 - 13_4$			206	12.9
257482.8	CH_3CN	$14_3 - 13_3$			157	13.4
257522.4	CH_3CN	$14_1 - 13_1$			100	13.9
257527.4	CH_3CN	$14_0 - 13_0$			93	14.0
257854.8	$HCOOCH_3$	$21_{17,4} - 20_{17,3}$	E		328	7.2
257864.8	$HCOOCH_3$	$21_{17,5} - 20_{17,4}$	E		328	7.2
258001.1 – 258007.2	$HCOOCH_3$	$21_{15,6} - 20_{15,5}$	A and E		285	10.3
258142.1	$HCOOCH_3$	$21_{14,8} - 20_{14,7}$	E		266	11.7
258152.9	$HCOOCH_3$	$11_{5,7} - 10_{4,6}$	E		56	4.8
258157.0	$HC^{15}N$	3 – 2			12	3.0
258255.8	SO	$6_6 - 5_5$			57	5.8
258275.0	$HCOOCH_3$	$21_{13,8} - 20_{13,7}$	E		248	13.0
258277.2	$HCOOCH_3$	$21_{13,8} - 20_{13,7}$	A		248	13.0
258277.2	$HCOOCH_3$	$21_{13,9} - 20_{13,8}$	A		248	13.0
258296.2	H_2CO	$10_{2,8} - 11_{0,11}$			241	
258296.2	$HCOOCH_3$	$21_{13,9} - 20_{13,8}$	E		248	13.0
258388.8	SO_2	$32_{4,28} - 32_{3,29}$			531	25.5
258480.6 – 258508.2	$HCOOCH_3$	23 – 22 and 21 – 20	A and E		155 – 456	150.9
258548.8 – 258549.3	CH_3OCH_3	$14_{1,14} - 13_{0,13}$	AA,AE,EE,EA		93	1.1
258667.0	SO_2	$20_{7,13} - 21_{6,16}$			313	2.5
258769.7	$HCOOCH_3$	$21_{11,11} - 20_{11,10}$	E		217	15.3
258780.4	CH_3OH	$19_3 - 19_2$	A+ –			
258942.2	SO_2	$9_{3,7} - 9_{2,8}$			63	4.6
259001.4	$HCOOCH_3$	$9_{3,7} - 8_{1,8}$	A		33	
259011.8	$H^{13}CN$	3 – 2			12	3.0
259128.4	$HCOOCH_3$	$21_{10,12} - 20_{10,11}$	A		203	16.3
259232.7	C_2H_5CN	$29_{3,27} - 28_{3,26}$			197	28.7
259273.7	CH_3OH	$17_2 - 16_1$	A –		836	
259275.5	$HCOOCH_3$	$34_{4,30} - 34_{4,31}$	A		366	1.0
259299.8	$HCOOCH_3$	$34_{4,30} - 34_{3,31}$	A		366	12.0
259308.0	U					
259341.9 – 259343.2	$HCOOCH_3$	24 – 23	A and E		158	184.8
259398.0	(U)					
259599.5	SO_2	$30_{4,26} - 30_{3,27}$			471	23.3
259617.2	$^{34}SO_2$	$13_{3,11} - 13_{2,12}$			105	6.9
259629.4	$HCOOCH_3$	$21_{9,12} - 20_{9,11}$	E		190	17.2
259646.8 – 259652.8	$HCOOCH_3$	21 – 20	A and E		190	51.6
259686.9	$HCOOCH_3$	$34_{5,30} - 34_{3,31}$	A		366	1.0
259725.3 – 259726.2	$HCOOCH_3$	28 – 28	A		225	6.0
259842.9 – 259847.4	C_2H_5CN	29 – 28			298 – 321	50.4
259862.8 – 259869.9	C_2H_5CN	29 – 28			277 – 347	50.2
260013.7	C_2H_5CN	29 – 28			436	21.2
260025.6	C_2H_5CN	$29_{7,22} - 28_{7,21}$			241	27.3
260081.1	C_2H_5CN	29 – 28			470	20.2
260192.0	CH_2CO	$13_{1,13} - 12_{1,12}$			101	12.9
260221.6	C_2H_5CN	$29_{6,24} - 28_{6,23}$			227	27.8
260229.2	C_2H_5CN	$29_{6,23} - 28_{6,22}$			227	27.8
260239.0	C_2H_5CN	29 – 28			545	17.8
260244.4	$HCOOCH_3$	$21_{3,18} - 20_{3,17}$	E		147	20.2
260255.2	$HCOOCH_3$	$21_{3,18} - 20_{3,17}$	A		147	20.2
260255.5	$H^{13}CO^+$	3 – 2			13	3.0
260314.0	(U)					
260327.0	$^{34}SO_2$	$24_{2,22} - 24_{1,23}$			292	12.2
260328.5	C_2H_5CN	$29_{19,11} - 28_{19,10}$			586	16.6
260381.6	CH_3OH	$20_3 - 20_2$	A+ –			
260384.2	$HCOOCH_3$	$21_{8,13} - 20_{8,12}$	E		180	18.0

TABLE 2. *(continued)*

ν_0 (MHz)	molecule	transition	symmetry state	values of F	E_u/k (K)	S_{ij}
260518.0	SiO	6 – 5			44	6.0
260535.7	C_2H_5CN	$29_{5,25}$ – $28_{5,24}$			215	28.1
260541.1	C_2H_5CN	$11_{4,8}$ – $10_{3,7}$			46	4.6
260549.0	$HCOOCH_3$	$9_{3,7}$ – $8_{0,8}$			33	0.1
260578.0	(U)					
260664.8	C_2H_5CN	$29_{4,26}$ – $28_{4,25}$			205	28.4
260667.1	C_2H_5CN	$11_{4,7}$ – $10_{3,8}$			46	4.6
260679.0	C_2H_5CN	$29_{5,24}$ – $28_{5,23}$			215	28.1
260681.5 – 260682.3	$HCOOCH_3$	20 – 20	A		190	18.0
260726.0	(U)					
260754.6 – 260761.7	CH_3OCH_3	$6_{3,3}$ – $5_{2,4}$	AA,AE,EE,EA		32	2.9
261148.9	$HCOOCH_3$	$21_{5,17}$ – $20_{5,16}$	E		154	19.8
261164.9	$HC^{17}O^+$	3 – 2			13	3.0
261165.4	$HCOOCH_3$	$21_{5,17}$ – $20_{5,16}$	A		154	19.8
261206.0	(U)					
261244.3 – 261250.2	CH_3OCH_3	$15_{5,10}$ – $15_{4,11}$	AA,AE,EE,EA		144	7.6
261263.4	$HN^{13}C$	3 – 2			25	3.0
261704.4	CH_3OH	12_6 – 13_5	E1			
261805.7	CH_3OH	2_1 – 1_0	E1			
261843.7	SO	7_6 – 6_5			48	7.0
261848.1	C_2H_5CN	$29_{12,17}$ – $30_{11,20}$			347	2.9
261951.9 – 261959.3	CH_3OCH_3	$15_{5,11}$ – $15_{4,12}$	AA,AE,EE,EA		144	7.6
262004.3	CCH	3, 7/2 - 2, 5/2		4 - 3	13	
262006.5	CCH	3, 7/2 - 2, 5/2		3 - 2	13	
262065.0	CCH	3, 5/2 - 2, 3/2		3 - 2	13	
262067.5	CCH	3, 5/2 - 2, 3/2		2 - 1	13	
262183.8	C_2H_5CN	$29_{4,25}$ – $28_{4,24}$			205	28.4
262222.9	C_2H_5CN	$6_{5,2}$ – $5_{4,1}$			37	4.6
262224.2	CH_3OH	21_3 – 21_2	A+ –			
262252.9	$HCOOCH_3$	$15_{10,6}$ – $15_{9,7}$	E		137	5.3
262256.9	SO_2	$11_{3,9}$ – $11_{2,10}$			83	5.8
262264.7	$HCOOCH_3$	$15_{10,5}$ – $15_{9,6}$	E		137	5.3
262388.6 – 262394.9	CH_3OCH_3	$13_{5,8}$ – $13_{4,9}$	AA,AE,EE,EA		118	6.4
262619.0	CH_2CO	$13_{2,12}$ – $12_{2,11}$			140	12.7
262882.9 – 262895.3	CH_3OCH_3	$12_{5,8}$ – $12_{4,9}$	AA,AE,EE,EA		106	5.7
262969.7	SO_2	$25_{8,18}$ – $26_{7,19}$			455	3.3
262999.0	CH_3OH	30_4 – 29_5	A–			
263043.6 – 263050.3	CH_3OCH_3	$11_{5,6}$ – $11_{4,7}$	AA,AE,EE,EA		95	5.1
263100.9 – 263113.7	CH_3OCH_3	$11_{5,7}$ – $11_{4,8}$	AA,AE,EE,EA		95	5.1
263400.7 – 263420.7	CH_3OCH_3	9_5 – 9_4	AA,AE,EE,EA		76	7.6
263436.5	$^{34}SO_2$	$34_{4,30}$ – $34_{3,31}$			593	26.7
263506.8 – 263519.0	CH_3OCH_3	$8_{5,3}$ – $8_{4,4}$	AA,AE,EE,EA		68	6.4
263516.2	C_2H_5CN	$30_{2,29}$ – $29_{2,28}$			202	29.8
263544.1	SO_2	$30_{3,27}$ – $30_{2,28}$			459	20.3
263578.3 – 263588.0	CH_3OCH_3	$7_{5,2}$ – $7_{4,3}$	AA,AE,EE,EA		61	5.0
263624.9 – 263634.3	CH_3OCH_3	$6_{5,1}$ – $6_{4,2}$	AA,AE,EE,EA		54	3.4
263653.3 – 263662.7	CH_3OCH_3	$5_{5,0}$ – $5_{4,1}$	AA,AE,EE,EA		49	1.8
263744.0	(U)					
263792.5	HC_3N	29 – 28			190	29.0
263810.8	C_2H_5CN	$29_{2,27}$ – $_{2}82,26$			195	28.8
264439.3	HC_3N	29 – 28 (ν_7=1, 1e)				29.0
264451.2	$H^{13}CCCN$	30 – 29			13	30.0
264694.0	(U)					
264744.0	CH_3OH	30_4 – 29_5	A+			
264747.9	C_2H_5CN	$30_{1,29}$ – $29_{1,28}$			202	29.8
264817.0	HC_3N	29 – 28 (ν_7=1, 1f)				29.0
265024.9	$HCOOCH_3$	$21_{6,15}$ – $20_{6,14}$	A		162	19.3
265176.0	(U)					
265200.0	(U)					
265289.7	CH_3OH	6_1 – 5_2	E1			
265482.2	SO_2	$34_{4,30}$ – $34_{3,31}$			594	27.1
265489.0	$^{34}SO_2$	$26_{4,22}$ – $26_{3,23}$			362	18.5
265554.1	$^{34}SO_2$	$7_{2,6}$ – $6_{1,5}$			35	2.7
265630.0	U					
265759.5	C_3H_2	$4_{4,1}$ – $3_{3,0}$	O		30	2.8
265886.2	HCN	3 – 2		2 - 1	13	3.0
265886.4	HCN	3 – 2		3 - 2	13	3.0
265886.5	HCN	3 – 2		4 - 3	13	3.0
266084.0	(U)					

TABLE 2. *(continued)*

ν_0 (MHz)	molecule	transition	symmetry state	values of F	E_u/k (K)	S_{ij}
266161.0	HDO	$2_{2,0} - 3_{1,3}$			157	0.1
266334.5	C_2H_5CN	8 – 9			87	0.1
266386.0	U					
266613.0	(U)					
266832.2	$HCOOCH_3$	$22_{4,19} - 21_{4,18}$	A		160	21.1
266838.1	CH_3OH	$5_2 - 4_1$,	E1			
266841.9	C_2H_5CN	$19_{3,17} - 18_{2,16}$			92	5.5
266951.7	C_2H_5CN	$15_{4,12} - 15_{2,13}$			69	
267197.8	SO	$3_4 - 4_3$			29	
267360.0	(U)					
267403.4	CH_3OH	$9_0 - 8_1$	E1			
267530.2	OCS	22 – 21			148	22.0
267537.4	SO_2	$13_{3,11} - 13_{2,12}$			106	6.9
267557.6	HCO^+	3 – 2			26	3.0
267620.0	(U)					
267627.9	$^{13}CH_3CN$	$15_8 - 14_8$			561	10.7
267642.3	NH_2D	$12_{5,8} - 12_{4,8}$			13	
267703.4	$^{13}CH_3CN$	$15_7 - 14_7$			454	11.7
267719.8	SO_2	$28_{4,24} - 28_{3,25}$			416	20.6
267869.3	$^{13}CH_3CN$	$15_4 - 14_4$			218	13.9
267871.1	$^{34}SO_2$	$15_{3,13} - 15_{2,14}$			132	7.9
267887.3	CH_3OH	$24_5 - 23_6$	E1			
267904.6	$^{13}CH_3CN$	$15_3 - 14_3$			167	14.4
267944.8	$^{13}CH_3CN$	$15_1 - 14_1$			110	14.9
267949.8	$^{13}CH_3CN$	$15_0 - 14_0$			103	15.0
268002.5	C_2H_5CN	$30_{3,28} - 29_{3,27}$			210	29.7
268168.4	SO_2	$9_{5,5} - 10_{4,6}$			103	0.8
268552.7	$HCOOCH_3$	$23_{2,21} - 22_{2,20}$	E		165	22.3
268561.2	$HCOOCH_3$	$23_{2,21} - 22_{2,20}$	A		165	22.3
268803.1 – 268803.9	C_2H_5CN	30 – 29			311 – 334	52.7
268824.3 – 268828.8	C_2H_5CN	30 – 29			290 – 360	52.5
268860.2	C_2H_5CN	$30_{13,18} - 29_{13,17}$			387	24.4
268875.3	$HCOOCH_3$	$8_{4,5} - 7_{2,6}$	A		32	
268892.5	C_2H_5CN	$30_{8,23} - 29_{8,22}$			271	27.9
268908.6	C_2H_5CN	$30_{14,16} - 29_{14,15}$			417	23.5
268967.7	C_2H_5CN	$30_{15,16} - 29_{15,15}$			449	22.5
269015.1	C_2H_5CN	$30_{7,24} - 29_{7,23}$			254	28.4
269036.2	C_2H_5CN	$30_{16,14} - 29_{16,13}$			483	21.5
269069.1 – 269093.8	$HCOOCH_3$	24 – 23	A and E		168	171.2
269234.6	C_2H_5CN	$30_{6,25} - 29_{6,24}$			240	28.8
269245.4	C_2H_5CN	$30_{6,24} - 29_{6,23}$			240	28.8
269933.1 – 269934.2	$HCOOCH_3$	25 – 24	A and E		171	192.8
270013.1	$HCOOCH_3$	22 – 21	A		441	3.9
270501.5 – 270503.4	$HCOOCH_3$	22 – 21	A and E		279	26.2
270520.8	H_2CS	$8_{1,8} - 7_{1,7}$			72	7.9
270598.0	(U)					
270664.0	U					
270681.3 – 270683.8	$HCOOCH_3$	22 – 21	A		262	28.6
271229.3	$HCOOCH_3$	$22_{11,11} - 21_{11,10}$	E		259	
271240.2	$HCOOCH_3$	$22_{11,12} - 21_{11,11}$	A		230	16.5
271246.2	CH_3OCH_3	$14_{10,5} - 15_{9,6}$	EA		236	
271251.3	CH_3OCH_3	$14_{10,5} - 15_{9,6}$	EE		236	
271253.1	$HCOOCH_3$	$22_{11,12} - 21_{11,11}$	E		230	16.5
271277.5	CH_3OCH_3	$14_{10,4} - 15_{9,7}$	EA		236	
271312.0	(U)					
271410.2	$^{34}SO_2$	$17_{2,16} - 17_{1,17}$			148	5.4
271505.9	$HCOOCH_3$	$21_{5,16} - 20_{5,15}$	E		155	19.9
271506.6	C_2H_5CN	$30_{4,26} - 29_{4,25}$			218	29.5
271524.7	$HCOOCH_3$	$21_{4,17} - 20_{4,16}$	E		151	20.2
271529.0	SO_2	$7_{2,6} - 6_{1,5}$			36	2.7
271532.8	$HCOOCH_3$	$21_{5,16} - 20_{5,15}$	A		156	19.9
271544.8	$HCOOCH_3$	$21_{4,17} - 20_{4,16}$	A		152	20.2
271981.1	HNC	3 – 2			26	3.0
272028.0	(U)					
272849.9	$OC^{34}S$	23 – 22			157	23.0
272864.5	$HCOOCH_3$	$23_{3,20} - 22_{4,19}$	E		173	11.1
272884.9	HC_3N	30 – 29			203	30.0
272885.3	$HCOOCH_3$	$23_{3,20} - 22_{4,19}$	A		173	11.1

TABLE 3. *Observed line parameters from the JCMT observations of the OMC1 core.*
$T_R^*(\max)$ *is the antenna temperature of the line peak, and FWHM is the full width at half -maximum intensity. No corrections have been made for blending of transitions of different molecules, or blending of components from different sub-sources. Where transitions occur in close blends,* $T_R^*(\max)$ *is given in brackets, and FWHM is omitted. The rms error on* $T_R^*(\max)$ *is* ~ 0.5 K, *and the errors in the FWHM are of the order of the* 2.2 km s^{-1} *channel width. In Table 3.6, unidentified transitions are denoted by* U *or* (U), *as in Table 2, and the line rest frequencies are uncertain by* $\lesssim 8$ MHz.

TABLE 3.1. *Silicon- and sulphur-bearing species.*

molecular species	ν_0 (MHz)	$T_R^*(\max)$ (K)	FWHM (kms^{-1})
SiO	260518.0	26.4	28
^{29}SiO	257255.0	(5.5)	
^{13}CS	231220.8	6.7	8
SO	258255.8	45.0	~ 28
SO	261843.7	31.4	~ 23
SO	267197.8	6.3	11
SO_2	229347.7	6.0	8
SO_2	237068.8	(6.4)	
SO_2	238992.6	0.9	3
SO_2	257100.0	14.9	~ 12
SO_2	258388.8	3.3	14
SO_2	258667.0	2.9	9
SO_2	258942.2	(4.7)	
SO_2	259599.5	7.0	7
SO_2	262256.9	13.6	18
SO_2	262969.7	1.4	4
SO_2	263544.1	5.4	14
SO_2	265482.2	(3.2)	
SO_2	267537.4	(19.5)	
SO_2	267719.8	4.9	11
SO_2	268168.4	3.9	~ 26
SO_2	271529.0	12.1	24
$^{34}SO_2$	237170.3	(2.7)	
$^{34}SO_2$	259617.2	6.0	8
$^{34}SO_2$	260327.0	(2.0)	
$^{34}SO_2$	263436.5	1.1	5
$^{34}SO_2$	265554.1	1.3	~ 9
$^{34}SO_2$	267871.1	(2.3)	
$^{34}SO_2$	271410.2	2.3	2
OCS	231061.0	11.2	5
OCS	267530.2	(19.5)	
$OC^{34}S$	272849.9	1.3	2

TABLE 3.2. *Linear species.*

molecular species	ν_0 (MHz)	$T_R^*(\max)$ (K)	FWHM (kms^{-1})
$HC^{15}N$	258157.0	12.7	14
$H^{13}CN$	259011.8	13.4	16
HCN	265886.4	28.1	28
$HN^{13}C$	261263.4	(3.2)	
HNC	271981.1	8.5	4
HC_3N	263792.5	13.2	7
HC_3N	264439.3	3.6	
HC_3N	264817.0	3.9	7
HC_3N	272884.9	(5.6)	
CCH	262004.3	4.2	~ 4
CCH	262065.0	3.0	~ 4

TABLE 3.3. *Complex oxygen-bearing species.*

molecular species	ν_0 (MHz)	$T_R^*(\max)$ (K)	FWHM (kms^{-1})
CH_3OH	231281.1	6.3	5
CH_3OH	257402.2	(6.8)	
CH_3OH	258780.4	4.7	5
CH_3OH	259273.7	(3.3)	
CH_3OH	260381.6	(0.9)	
CH_3OH	261704.4	1.3	3
CH_3OH	262224.2	(2.4)	
CH_3OH	262999.0	0.9	7
CH_3OH	264744.0	(4.0)	
CH_3OH	265289.7	5.6	7
CH_3OH	266838.1	(10.3)	
CH_3OH	267403.4	10.6	7
CH_3OH	267887.3	1.0	
CH_3OCH_3	258548.8	2.9	
CH_3OCH_3	260754.6	1.6	
CH_3OCH_3	261244.3	(5.0)	
CH_3OCH_3	261951.9	2.2	
CH_3OCH_3	262388.6	2.8	
CH_3OCH_3	262882.9	3.6	
CH_3OCH_3	262895.3	2.5	
CH_3OCH_3	263043.6	1.9	1
CH_3OCH_3	263050.0	3.3	2
CH_3OCH_3	263100.9	1.6	
CH_3OCH_3	263107.2	2.9	
CH_3OCH_3	263400.7	(4.2)	
CH_3OCH_3	263506.8	4.8	
CH_3OCH_3	263511.7	5.7	
CH_3OCH_3	263578.3	6.0	
CH_3OCH_3	263624.9	3.7	
CH_3OCH_3	263653.3	1.8	
CH_3OCH_3	271246.2	(1.5)	

TABLE 3. *(continued)*

TABLE 3.3. *(continued) Complex oxygen-bearing species.*

molecular species	ν_0 (MHz)	T_R^*(max) (K)	FWHM (kms^{-1})
$HCOOCH_3$	229260.2	(2.8)	
$HCOOCH_3$	229319.2	(1.5)	
$HCOOCH_3$	229388.9	0.8	3
$HCOOCH_3$	229405.0	2.8	2
$HCOOCH_3$	229420.2	4.3	5
$HCOOCH_3$	229590.4	5.0	3
$HCOOCH_3$	231232.1	(2.0)	
$HCOOCH_3$	231315.4	(6.5)	
$HCOOCH_3$	231412.2	0.5	8
$HCOOCH_3$	237297.0	2.5	2
$HCOOCH_3$	237306.0	2.6	3
$HCOOCH_3$	237344.9	(2.3)	
$HCOOCH_3$	237393.2	(2.1)	
$HCOOCH_3$	237430.9	2.5	5
$HCOOCH_3$	257252.6	(5.5)	
$HCOOCH_3$	257854.8	1.8	
$HCOOCH_3$	257864.8	1.9	
$HCOOCH_3$	258001.2	2.6	6
$HCOOCH_3$	258296.2	(2.5)	
$HCOOCH_3$	258499.1	4.2	
$HCOOCH_3$	258769.7	0.6	5
$HCOOCH_3$	259128.4	1.4	3
$HCOOCH_3$	259275.5	(3.5)	
$HCOOCH_3$	259341.9	6.3	2
$HCOOCH_3$	259629.4	(3.3)	
$HCOOCH_3$	259646.8	2.3	
$HCOOCH_3$	259686.9	2.2	
$HCOOCH_3$	259725.3	1.4	3
$HCOOCH_3$	260244.4	(1.2)	
$HCOOCH_3$	260255.2	(2.5)	
$HCOOCH_3$	260384.2	(0.9)	
$HCOOCH_3$	260681.5	(3.2)	
$HCOOCH_3$	261148.9	3.0	5
$HCOOCH_3$	261165.4	(1.8)	
$HCOOCH_3$	263407.8	(4.2)	
$HCOOCH_3$	265024.9	1.7	5
$HCOOCH_3$	266832.2	(10.3)	
$HCOOCH_3$	268552.7	1.3	
$HCOOCH_3$	268561.2	0.8	
$HCOOCH_3$	269078.0	1.8	
$HCOOCH_3$	269933.1	4.3	2
$HCOOCH_3$	270013.1	1.5	2
$HCOOCH_3$	270501.5	1.7	
$HCOOCH_3$	270681.3	1.9	
$HCOOCH_3$	271229.3	2.1	7
$HCOOCH_3$	271253.1	(1.5)	
$HCOOCH_3$	272864.5	2.4	3
$HCOOCH_3$	272885.3	(5.6)	

TABLE 3.4. *Complex nitrogen-bearing species.*

molecular species	ν_0 (MHz)	T_R^*(max) (K)	FWHM (kms^{-1})
CH_3CN	238912.7	0.7	3
CH_3CN	238972.4	2.5	10
CH_3CN	239022.9	2.9	5
CH_3CN	239064.3	2.0	8
CH_3CN	239096.5	(0.5)	
CH_3CN	239119.5	(4.8)	
CH_3CN	239133.3	(7.5)	
CH_3CN	257210.7	(4.8)	
CH_3CN	257284.8	2.7	2
CH_3CN	257349.1	4.6	3
CH_3CN	257403.6	(6.8)	
CH_3CN	257448.1	(4.5)	
CH_3CN	257482.8	(3.8)	
CH_3CN	257522.4	10.0	
$^{13}CH_3CN$	267627.9	(1.5)	
$^{13}CH_3CN$	267869.3	(2.3)	
$^{13}CH_3CN$	267904.6	1.0	5
$^{13}CH_3CN$	267944.8	1.0	2
C_2H_5CN	229265.2	(2.8)	
C_2H_5CN	231310.4	(6.5)	
C_2H_5CN	237170.4	(2.7)	
C_2H_5CN	237338.1	(2.3)	
C_2H_5CN	237405.2	(1.8)	
C_2H_5CN	237476.1	0.7	5
C_2H_5CN	257239.9	(3.9)	
C_2H_5CN	259232.7	3.8	13
C_2H_5CN	259842.9	3.0	9
C_2H_5CN	259862.8	1.2	5
C_2H_5CN	260013.7	(3.3)	
C_2H_5CN	260025.6	(3.3)	
C_2H_5CN	260081.1	0.8	
C_2H_5CN	260221.6	3.3	
C_2H_5CN	260229.2	3.6	
C_2H_5CN	260328.5	(2.0)	
C_2H_5CN	260664.8	3.3	
C_2H_5CN	260679.0	(3.2)	
C_2H_5CN	261257.4	(4.0)	
C_2H_5CN	262183.8	2.8	3
C_2H_5CN	262222.9	(2.4)	
C_2H_5CN	263516.2	(5.7)	
C_2H_5CN	263810.8	1.9	
C_2H_5CN	264747.9	(4.0)	
C_2H_5CN	266334.5	8.0	2
C_2H_5CN	266951.7	1.8	2
C_2H_5CN	268002.5	2.7	11
C_2H_5CN	268803.1	2.8	
C_2H_5CN	268824.3	3.7	
C_2H_5CN	268860.2	2.8	
C_2H_5CN	268892.5	4.0	8
C_2H_5CN	268908.6	2.8	9
C_2H_5CN	268967.6	1.0	3
C_2H_5CN	269015.1	3.3	7
C_2H_5CN	269036.2	0.5	2

TABLE 3. *(continued)*

TABLE 3.5. *Miscellaneous species.*

molecular species	ν_0 (MHz)	T_R^*(max) (K)	FWHM (kms^{-1})
$H^{13}CO^+$	260255.4	(2.5)	
$HC^{17}O^+$	261164.9	(1.8)	
HCO^+	267557.6	(26.9)	~ 4
HDO	266161.0	2.5	12
NH_2D	267642.3	2.6	~ 18
C_3H_2	265759.5	2.4	~ 5
H_2CS	270520.8	3.6	4
CH_2CO	260192.0	0.8	2
CH_2CO	262619.0	0.6	2
H_2CO	258296.2	(2.5)	

TABLE 3.6. *Unidentified transitions.*

molecular species	ν_0 (MHz)	T_R^*(max) (K)	FWHM (kms^{-1}))
(U)	231266.0	1.2	3
(U)	231342.0	1.0	~ 5
(U)	237288.0	2.0	3
(U)	239046.0	1.3	3
(U)	257188.0	3.5	7
U	259308.0	2.8	7
(U)	259398.0	0.8	5
(U)	260314.0	1.9	2
(U)	260578.0	1.3	3
(U)	260726.0	1.6	5
(U)	261206.0	2.0	7
(U)	263744.0	2.8	8
(U)	264694.0	6.7	5
(U)	265176.0	2.0	5
(U)	265200.0	2.6	12
U	265630.0	3.1	2
(U)	266084.0	8.6	14
U	266386.0	3.5	9
(U)	266613.0	1.1	7
(U)	267360.0	2.8	13
(U)	267620.0	4.1	9
(U)	270598.0	3.2	1
U	270664.0	4.7	2
(U)	271312.0	1.8	5
(U)	272028.0	4.9	9

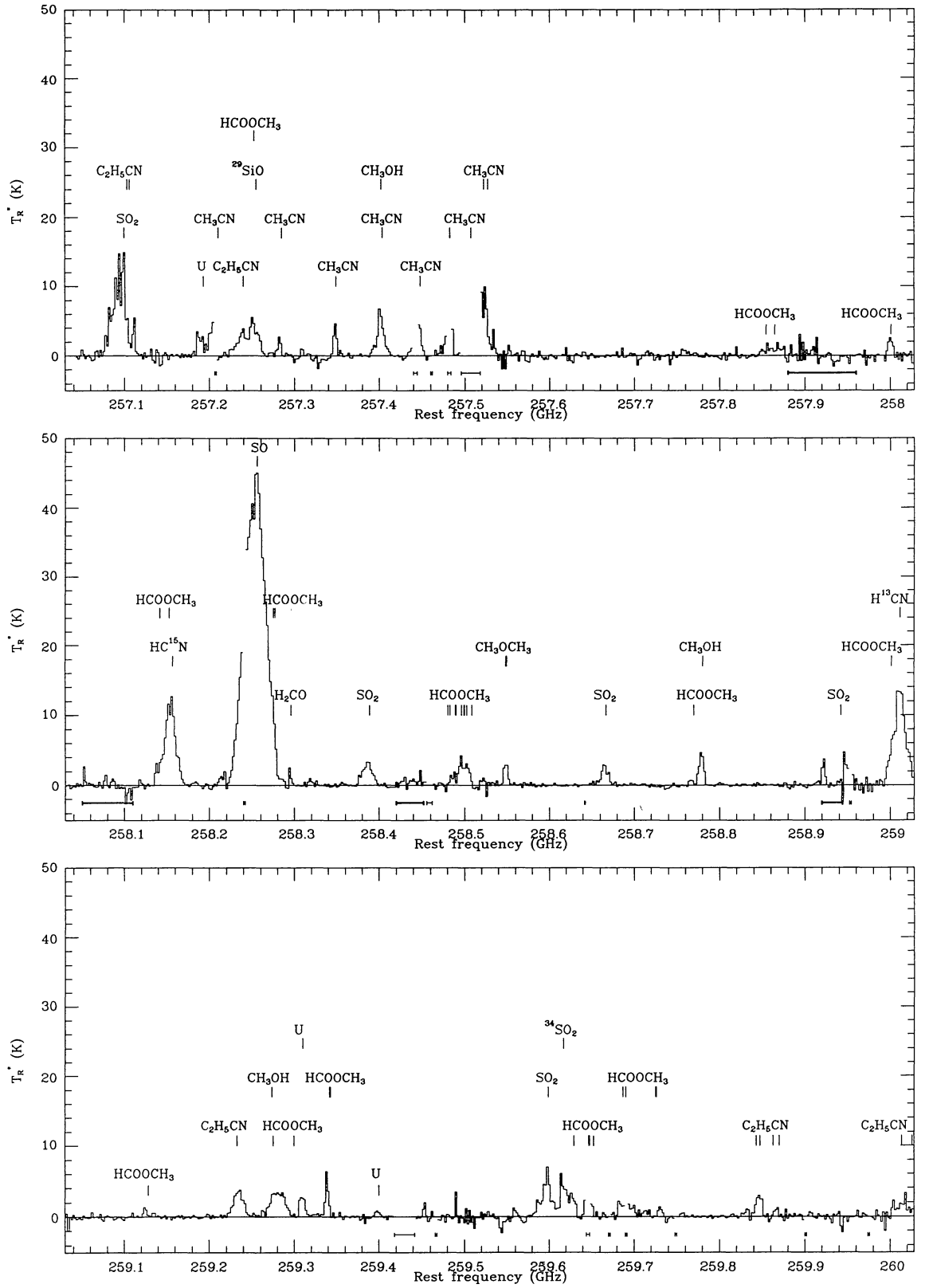

FIGURE 1a. The single-sideband spectra towards the OMC1 cloud core. The scales are rest frequency (in a reference frame with v_{lsr} = 9 km s^{-1}), and corrected antenna temperature T_R^*, as described in the text. The channel widths are 2.0 MHz. Thin bars under a portion of the spectrum indicate a gap where the DSB data could not be deconvolved, and thick bars indicate a region where the deconvolution has resulted in spikes. a) The 257 – 273 GHz spectrum. b) Spectra in the 229 – 239 GHz region.

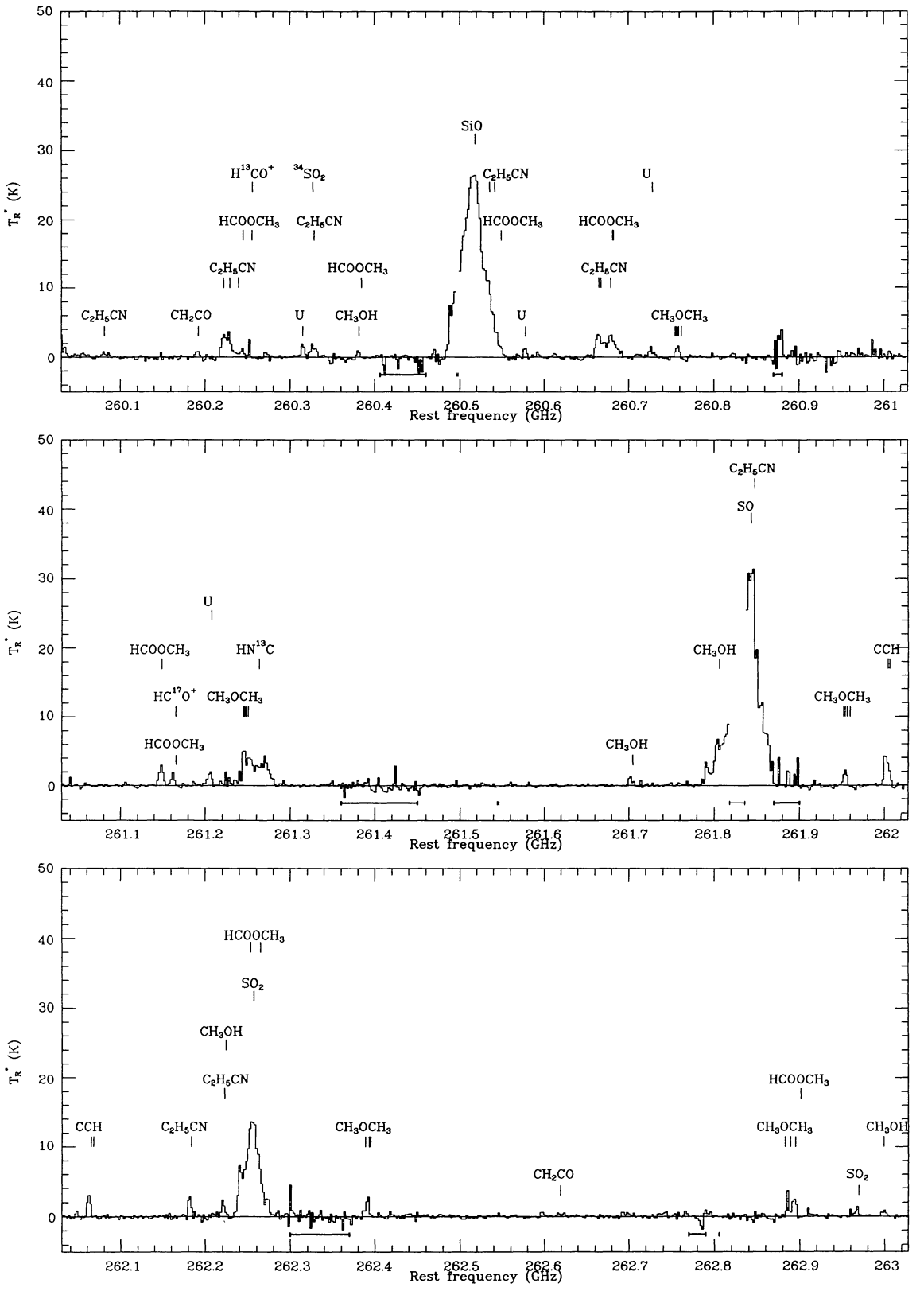

FIGURE 1a. (*continued*)

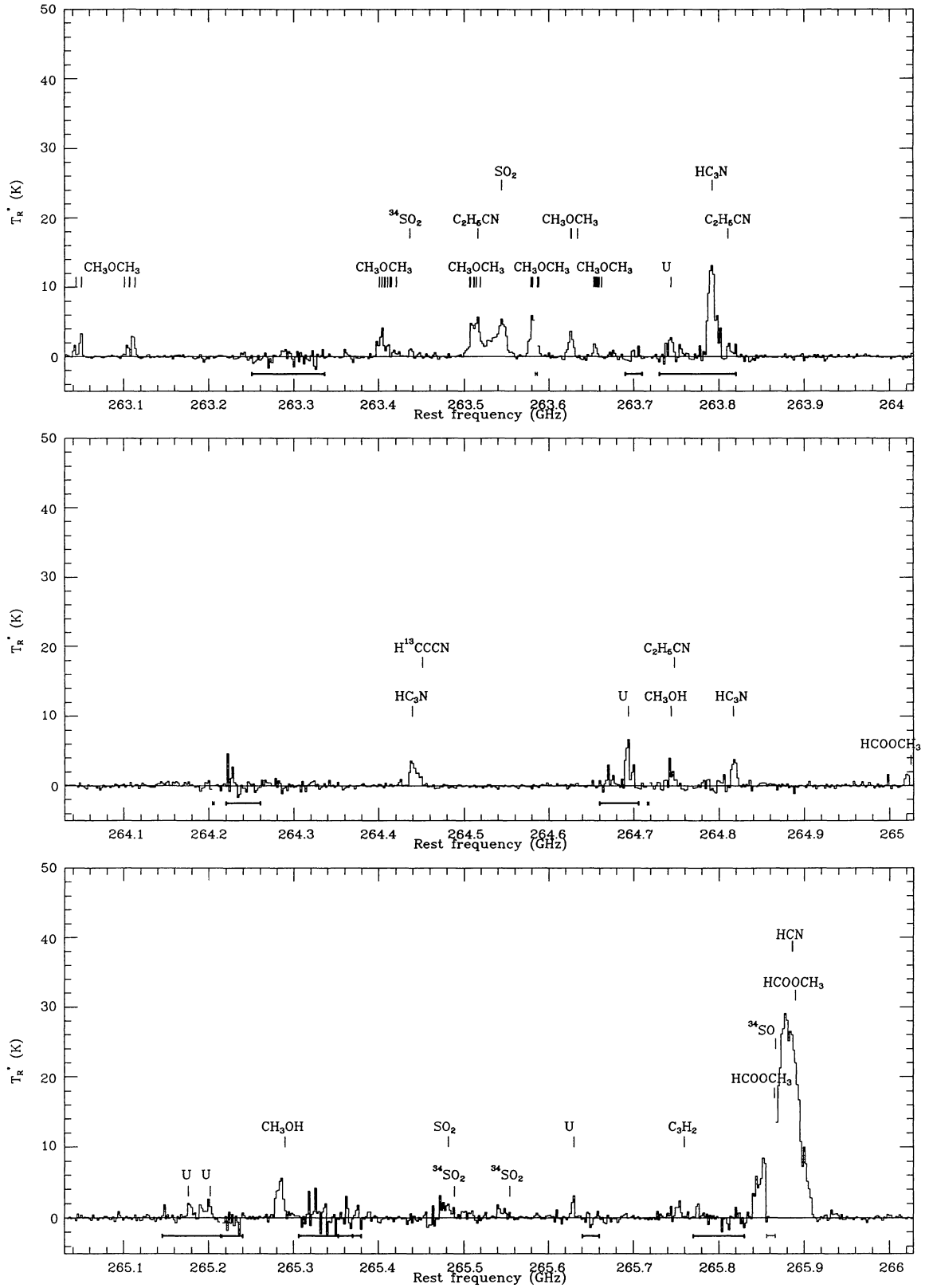

FIGURE 1a. (*continued*)

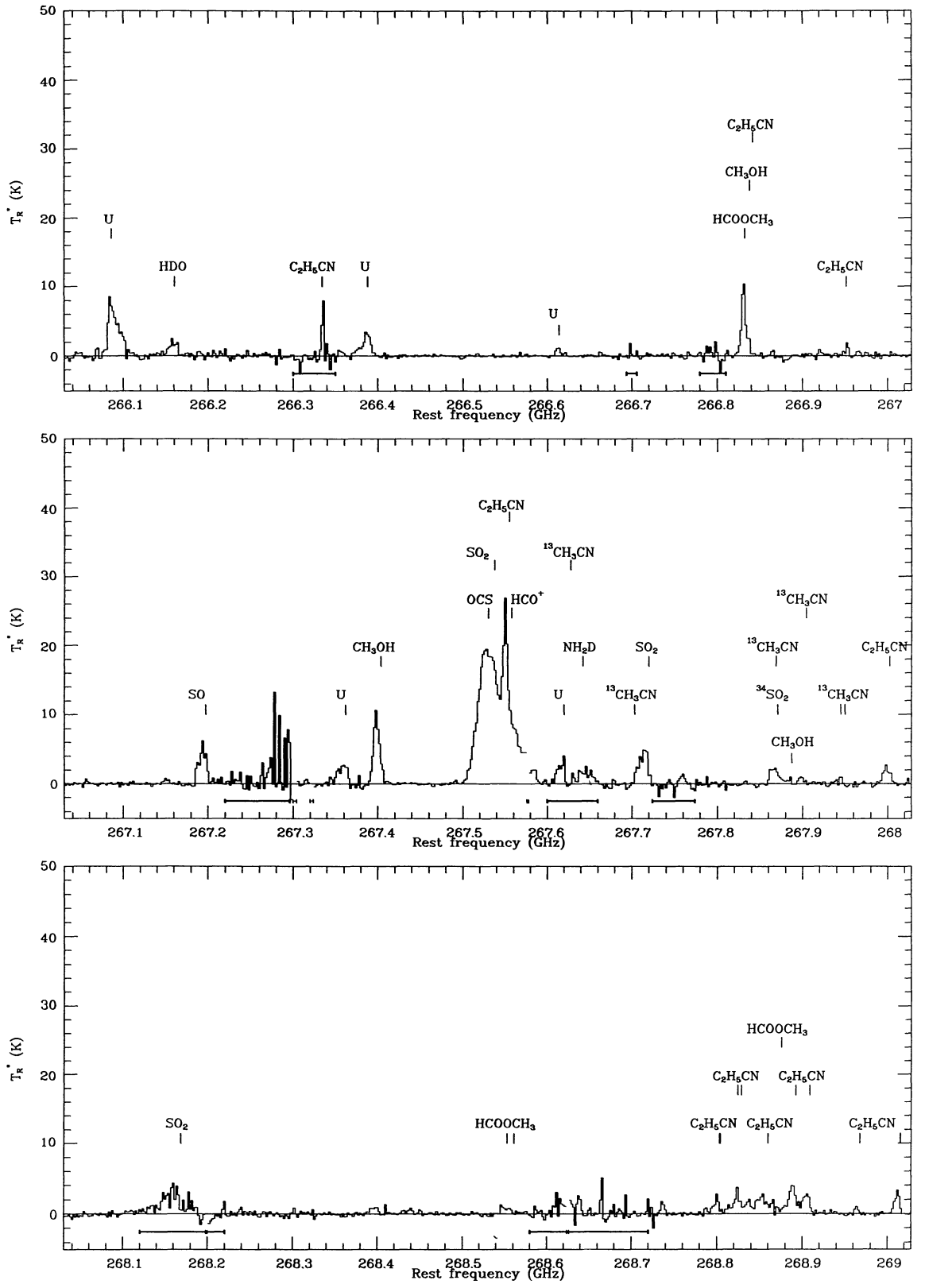

FIGURE 1a. (*continued*)

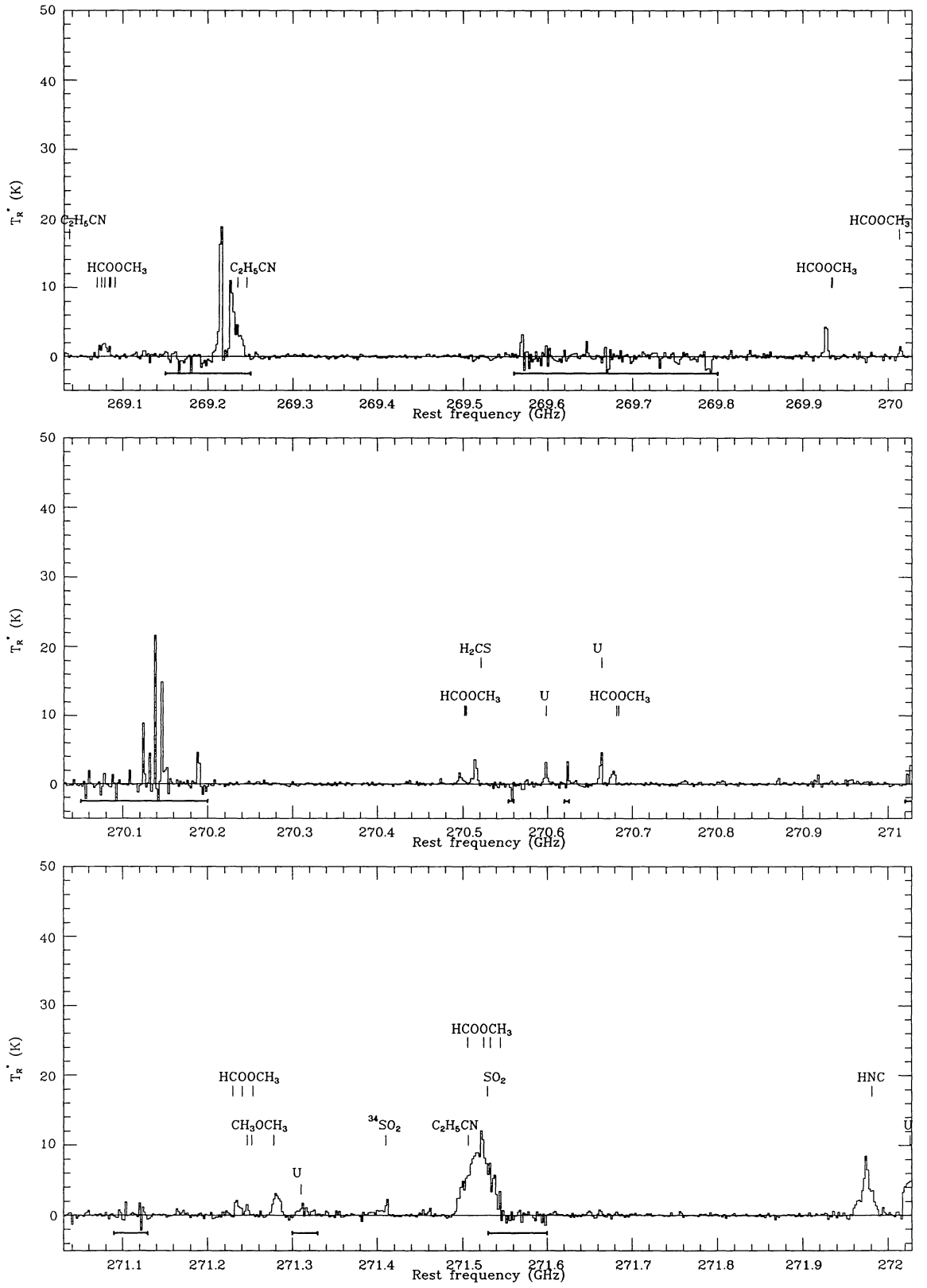

FIGURE 1a. (*continued*)

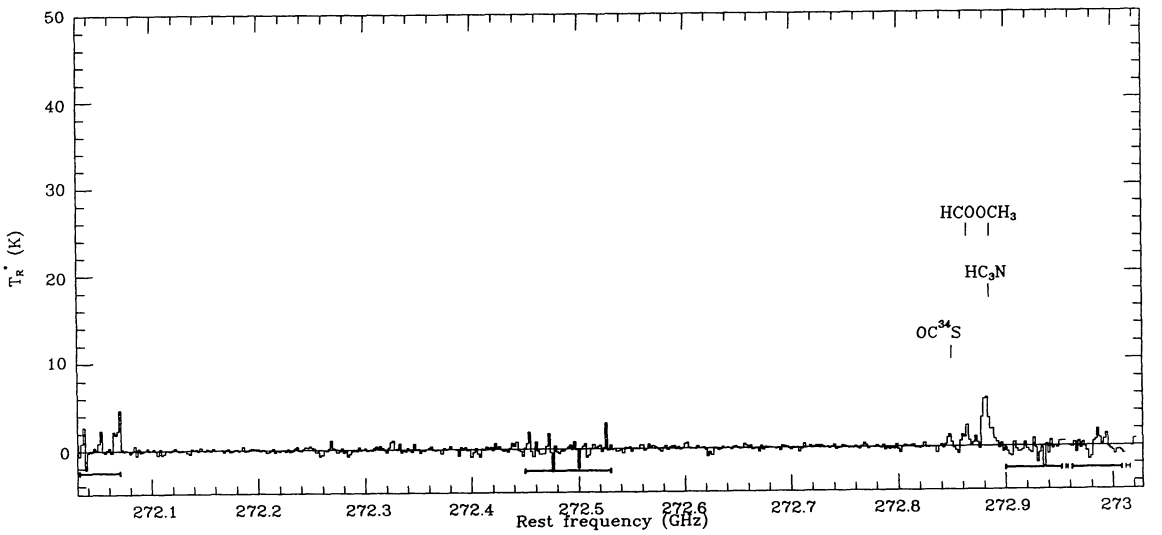

FIGURE 1a. (*continued*)

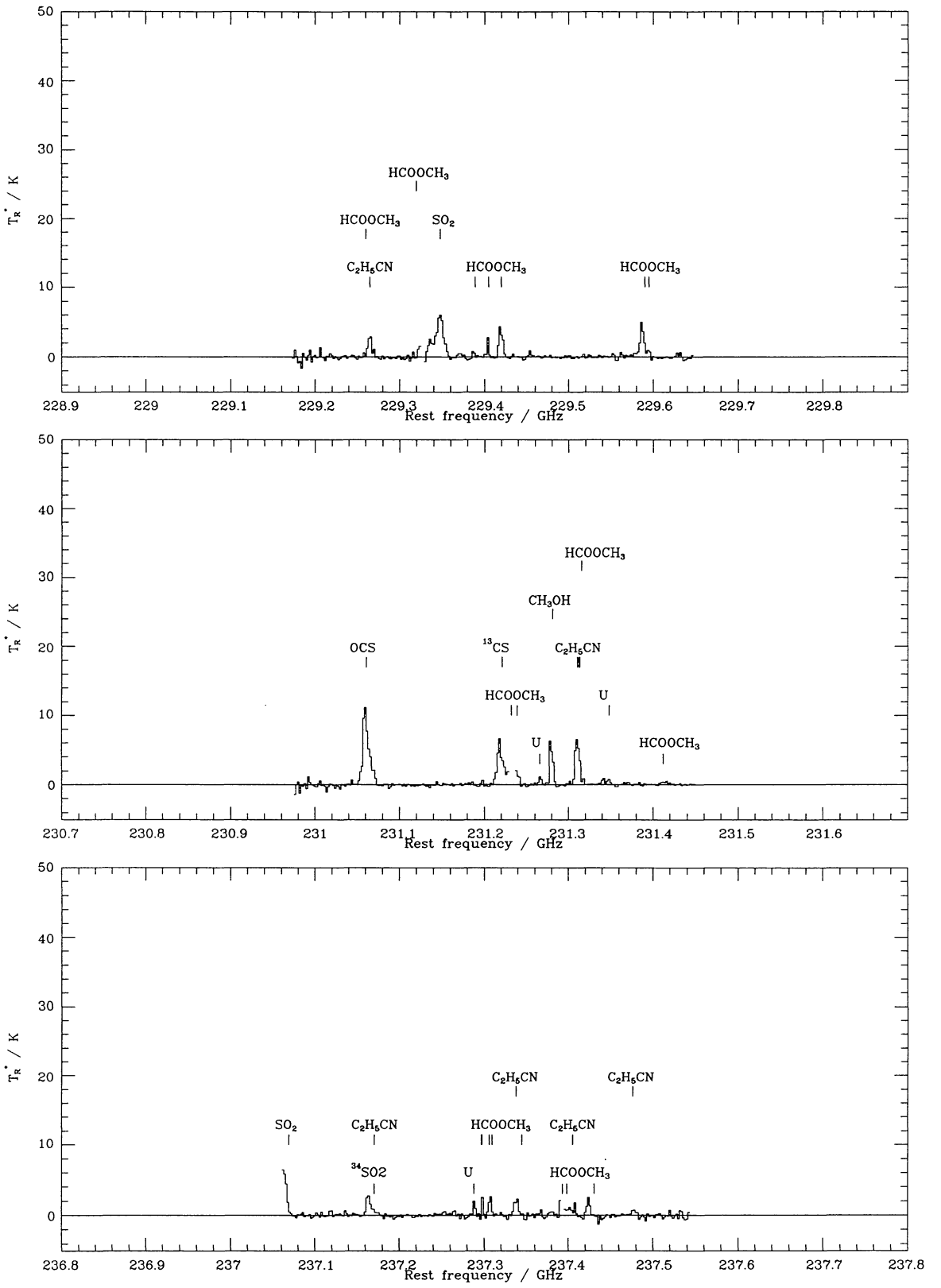

FIGURE 1b.

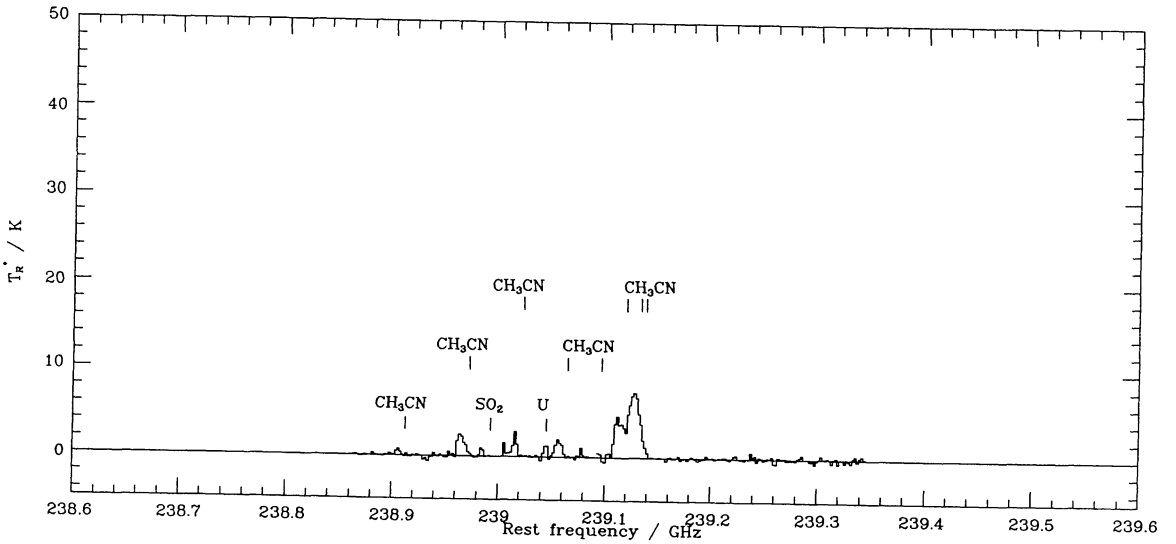

FIGURE 1b. (*continued*)

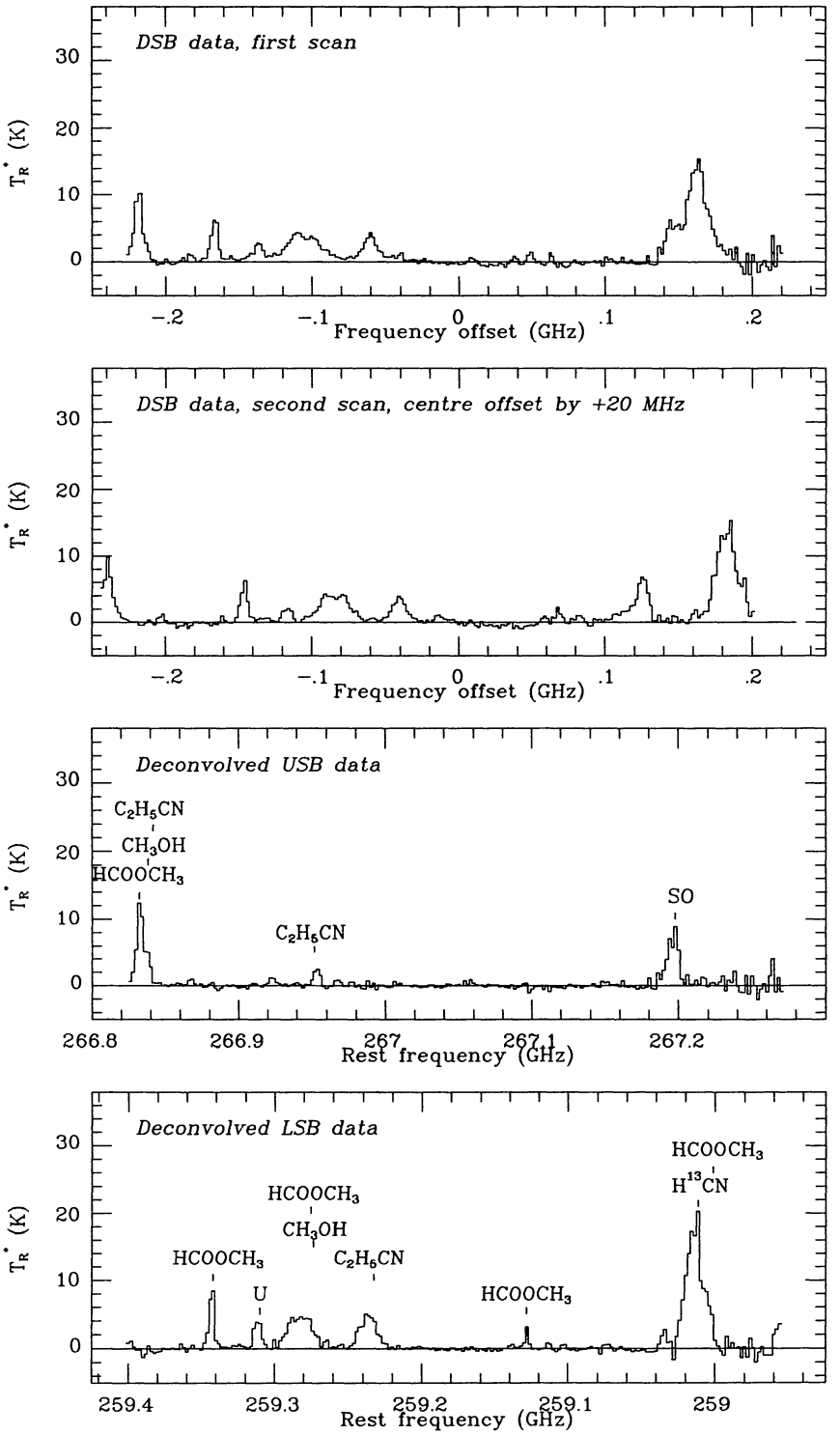

FIGURE 2. Examples of the deconvolution from double-sideband to single-sideband data. The top two spectra spectra show a DSB scan, observed with and without a shift in the centre frequency. The horizontal scale is the frequency offset from the passband centre. The 40 MHz shift between lower and upper sideband lines is clearly visible. The bottom two spectra show the devonvolved LSB and USB data. The rest frequency scales have been plotted such that LSB and USB lines lie directly below the corresponding DSB features in the top spectrum.

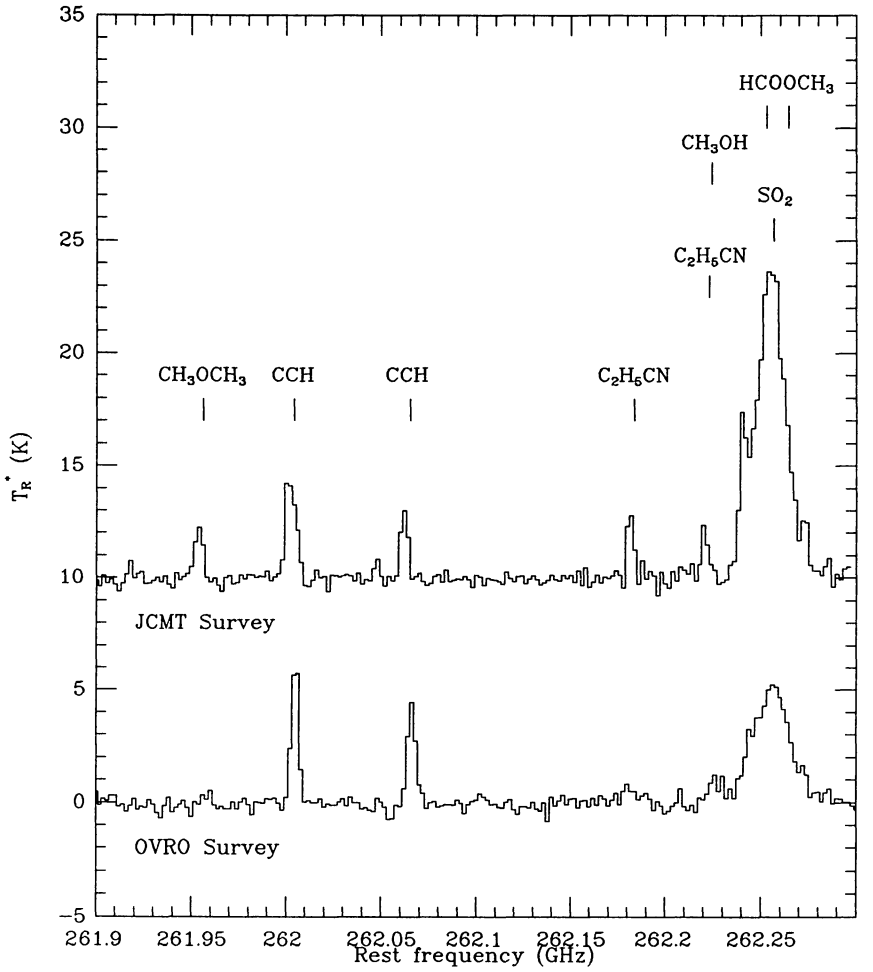

FIGURE 3. Examples of lines observed in both the JCMT and the OVRO surveys. The relative line strengths vary from $R_{J:O} = 0.7$ for CCH to $R_{J:O} \gtrsim 4.5$ for CH_3OCH_3, where $R_{J:O} = T_R^*(\text{max})$ (JCMT) / $T_R^*(\text{max})$ (OVRO).